MAX-PLANCK-GESELLSCHAFT
ZUR FÖRDERUNG DER WISSENSCHAFTEN E.V.
PROJEKTGRUPPE FÜR LASERFORSCHUNG
D-8046 GARCHING bei München/Germany

Target Experiments with Asterix III

K. Eidmann, G. Brederlow, P. Brodmann, R. Sigel,
R. Volk, S. Witkowski, K.J. Witte

PLF 4 January 1978

Errata

The equation on page 8 should read:

$$\Phi_{max} = 10^{14} \, (kT_{hot})^{3/2} \quad \frac{W}{cm^2}$$

The correct formula presented on fig. 14 is $kT_{hot} \propto \Phi_{abs}^{2/3}$

Diese Arbeit wurde gefördert durch das Bundesministerium für Forschung und Technologie und durch Euratom.

PLF 4 / 1978

Target Experiments with Asterix III *)

January, 1978

Abstract

Results from the initial target shots with the iodine laser Asterix III at a power of 0.3 TW (100 J/300 ps) on target are presented. Several points of importance for reliable target experiments as the focussability, the stability of the focus position, the prepulse mainpulse contrast, and the isolation of the laser against reflected light have been studied. In addition we present preliminary results on the reflection of laser light and the emitted X-radiation from plane solid targets at normal and oblique incidence.

---

*) Presented at the 11th European Conference on Laser Interaction with Matter, Oxford, 19. - 23. September, 1977.

1. Introduction

The high power iodine laser (λ = 1.3 µm) /1/ has been developed mainly for laser fusion application. Target experiments with "Plasterix" at a moderate power level of 30 GW have demonstrated that this type of laser can be successfully operated together with a target /2/. Meanwhile the reliability of "Asterix III" /3/, which has produced laser pulses of 1 TW, has been sufficiently increased to start target experiments at higher powers. Results of a first series of about 100 target shots are described in this report.

2. Experimental Setup

The experimental setup is shown in fig. 1. The laser beam of 18 cm diameter is focussed by an aspherical f/2 lens on plane massive targets of plexiglass or steel. To change the focus position the lens was axially moved, whereas the target was in a fixed position, which was controlled by imaging the target on a screen. Calorimeter measure the incident energy and the energy reflected back through the lens. A fast streak camera with an S1 cathode is used for measurement of the pulse duration directly at λ = 1.3 µm. The prepulse mainpulse contrast is controlled routinely in each shot by a photomultiplier (risetime ~ 3 ns) with an S1 cathode. A Fabry Perot spectrometer with an IR-Vidicon as a detector measures the spectrum

of the reflected light. The light scattered into the total solid angle is measured by an Ulbricht-sphere with Ge-diodes /5/. Information on the X-ray spectrum in the energy region 1 to 20 keV is obtained by the absorbing foil method /4/. In some shots a pinhole camera has been used to give X-ray pictures of the plasma.

3. Incident Beam Characterisation

During the first series of target shots described in this report the energy on target was restricted to 100 J, because only one half of the final amplifier of Asterix III was available. Typical pulse durations of 300 ps have been measured, see fig. 2. Thus the maximum incident power was 0.3 TW. From the measurement of the incident beam divergence /3/, which is 4 to 5 times the diffraction limited value, and from the quality of the used f/2 lens a spot size of 50 µm for half energy was estimated, yielding intensities up to 10^{16} W/cm^2 in the focus.

An excellent prepulse mainpulse contrast has been found. The largest energy of modelockpulses passing the closed pulsecutter before the mainpulse was about 1 µJ at the output of the laser. Contributions due to amplified spontaneous emission and self-oscillations /2/ are less than 100 W during the time of flash-lamp ignition until the laserpulse passes the laserchain, which is about 10 µs. The target did not influence the prepulse behaviour, even if a target with a well polished highly reflecting metal surface was carefully aligned in the focus at

normal incidence. The found favourable prepulse behaviour is attributed to the use of a saturable absorber and a high contrast pulse cutting system in the laserchain.

4. Position of the Focus

Since at present no oscillator with a high repetition rate exists, a reliable method to find the axial position of the focus in a few shots is necessary. That can be done by using a plate with holes (Hartmannplate) in front of the focussing lens and producing a picture on burn paper near the focus, see fig. 3. An example of a burn obtained with 1 cm diameter holes in the Hartmannplate is shown in fig. 4. In this particular case, due to misalignment, the laser beam was not homogenous over its crossection giving different bright spots. Even in this case the distance between the spots d can be determined with a good accuracy ($\pm$ 5 µm). Fig. 5 shows the variation of the spot separation d with the distance between the lens and the burn paper demonstrating the high accuracy of this method. A useful, practical way to determine the axial focal position in two shots is to take one burn in front and one burn behind the focus and to determine the focus position from

$$a_1 = A \frac{d_1}{d_1 + d_2}$$

with $d_{1,2}$ the spot separations in both burnpaper positions, a_1 the distance between the focus and the burnpaper in position 1 and A the distance between the two burnpaper positions. The accuracy of this method is approximately given by

$$|\Delta a_1| \approx \frac{f}{R} |\Delta \alpha| + \frac{1}{2} |\Delta A|$$

where f is the focal length of the focussing lens and R the distance of the hole in the Hartmannplate from the axis. In the present experiment the determination of the axial position is accurate within ± 40 µm.

The described method has been routinely applied between several sequences of shots. It has been found that the focus remained within the measuring accuracy of ± 40 µm at the same position.

Craters on a steel target in focus and ± 300 µm out of focus are shown in fig. 6. The craters indicate a focal spot size less than 200 µm not in contradiction to the spot size (50 µm) expected from the divergence measurements. It is interesting that the structure of these craters is very similar to that of craters shown in fig. 7 produced with our Yag-laser system under similar conditions (f/2 lens, steel target, but lower laser energy, see /6/). We believe therefore, that the shape of such craters is useful to give indications for the beam quality of the laser.

X-ray pinhole pictures made with a tungsten target showed a hot plasma diameter not exceeding 100 µm.

5. Reflection Measurements

First we present some studies concerning the angular distribution of the scattered light at normal incidence. The reflection through the focussing f/2 lens did not exceed about 15%.

Detection of the scattered light on burnpaper positioned around the target inside the vacuum chamber showed, as known from Nd-laser experiments /7/, that the light scattered from the target is typically peaked around the target normal. This behaviour is also demonstrated by fig. 8, where we plotted the amount of light scattered from a plexiglass target into the focussing f/2 lens and into a lens viewing the target under an angle of 45° to the laser axis. The data are normalised to the incident energy and to the solid angles of the two lenses respectively, which are 0.2 for the f/2 focussing lens and 0.085 for the 45°-lens. The incident laser energy was between 70 and 110 J. Fig. 8 shows, that the intensity scattered into the focussing lens exceeds the intensity scattered into 45° by a factor of about 30 to 500 depending on the focus position. Typical for these measurements was a large scattering of the measured points, which are inside the hatched region in fig. 8.

To measure the total reflection losses, it is necessary to collect the light scattered into the total solid angle, which has been done with the Ulbrichtsphere. Using this technique we could also change the angle of incidence. At high intensities when the target was in focus, total reflections R_T up to 70% have been observed, where R_T is the sum of the light scattered into the Ulbrichtsphere and into the focussing lens. R_T depends only weakly on the intensity, see fig. 9, where the variation of R_T with the focus position at a fixed angle of incidence = 22.5° and a fixed laser energy of 30 J for a steel target

is plotted. We note that in our Yag-laser experiments the variation of the reflectance in the region of the focus depended on the laser pulse duration. For both, the reflection through the lens and the total reflection R_T, we observed there in the focus a minimum with short pulses (30 ps) /6/, but a maximum for long pulses (10 ns) /8/. In the restricted number of shots made with 300 ps iodine laser pulses the reflection showed a maximum near focus, see fig. 8 and 9, as it was typical for long pulses in the Yag-laser experiments.

The variation of R_T with the angle of incidence with the target in focus and out of focus respectively is shown in fig. 10. The E-vector of the incident light was in the plane of incidence (p - polarisation). With the target out of focus an indication of a minimum at about 30° is present, whereas with the target in focus R_T increases monotonically with increasing angle of incidence. A very similar behaviour has been found in a parallel experiment with our Yag-laser system using the same experimental technique /5/. We explain the minimum in the out of focus curve by resonance absorption contributing to the total absorption. The observation that the occurence of a minimum depends on the focus position is probably caused by geometry effects due to the different spot sizes in focus (50 µm) and out of focus (1000 µm) /5/. The backscattering into the focussing lens was at oblique incidence $\gtrsim$20° low and did not exceed a few %. These preliminary results will be completed by changing the incident light from p - to s - polarisation.

Initial measurements of the spectrum of the light scattered back through the focussing lens indicate a broadening of 5 to 10 Å. The broadening and also perhaps a shift, which has not yet been investigated by us, is of practical importance for the isolation of the laser against reflected light. It reduces the back-amplification of the reflected light /2/ in the laser amplifiers, whose bandwidth is less than 1 Å.

6. X-Ray Measurements

Simultaneously with the reflection the emitted X-ray continuum has been studied. Time and space integrated data are obtained by using plastic scintillators (2 mm thick NE 104) and absorbing foils (25, 51, 203 and 813 µm thick Be and 150 and 500 µm thick Al) for 6 energy channels within 1 to 20 KeV. Fig. 11 shows the variation of the soft X-ray signal 25 µm Be, $h\nu_{cutoff}$ = 1.4 KeV) and the hard X-ray signal (500 µm Al, $h\nu_{cutoff}$ = 16 KeV) with the target position at a constant laser energy of about 30 J. Fig. 11 demonstrates well the strong dependence of the hard X-ray signal on the intensity. In contrast to that the soft X-ray signal shows practically no variation over a large range of target positions. The dependence of the X-ray signals on the cutoff energy of the absorber foils for a high and a low incident intensity is presented in fig. 12. The curves show the expected typical non-thermal behaviour, see e.g. /9/. Values for T_{cold} and T_{hot} calculated from the slopes of curves like fig. 12 in the low and high energy region respectively are plotted in fig. 13 as a function of the incident

intensity, which was changed by moving the focussing lens. (In calculating these temperature values also the finite thickness of the scintillator has been taken into account, which is important for photon energies above 10 KeV). The values obtained for T_{cold} are low and depend only very weakly on the intensity. The hot temperatures range from 2 KeV to a few 10 KeV/11/. For high hot temperatures the measuring accuracy of the used setup is poor because the slope here depends only weakly on the temperature.

Since the absorbed intensity is known in this experiment from the Ulbrichtsphere measurements, we have also plotted T_{hot} versus the absorbed intensity for comparison with the flux limit, see fig. 14. The measured T_{hot} values are above values calculated from an unreduced Maxwellian flux limit which is for the λ= 1.3 µm iodine radiation at the critical density 5,9 x 10^{20} cm^{-3}

$$\Phi_{max} = 10^{14} \left(\frac{kT_{hot}}{KeV}\right)^{2/3} \quad \frac{W}{cm^2}$$

We note that the observed behaviour of the X-ray emission is well known from corresponding Nd- and CO_2 laser experiments and is essentially in agreement with results obtained there, see e.g. /10/, where a collection of data for T_{hot} from various laboratories is given.

Finally we mention that we have also measured the dependence of T_{hot} on the angle of incidence. The first results indicate an angular dependence, T_{hot} decreases with increasing angle of incidence, see fig. 15. The incident light was p-polarised. This

behaviour seems of interest for the absorption mechanism. Whether there exists a maximum for T_{hot} in the region 2o° to 30°, as one would expect from resonance absorption, is difficult to decide, due to the limited accuracy and the scattering of the data. More detailed measurements are planned in future experiments.

7. Conclusion

The main aspect of the present investigations was to get experience for the operation of the iodine laser with a target. As a reasonable procedure for that purpose we considered the reproduction of interaction experiments, the results of which were already known from corresponding Nd-laser experiments made in our and other laboratories. Nevertheless, the obtained results on reflection and X-ray emission are of interest for comparative considerations. However, the largest importance of the described experiments we see in the fact that the iodine laser system Asterix III fulfills now the conditions necessary for target experiments and that it was possible to obtain reproducible and reliable interaction results. New interaction studies at a power level up to 1 TW with the complete Asterix III system are possible in the future.

References

/1/ K. Hohla, K.L. Kompa, Handbook of Chemical Lasers, Chapt. 12. Edited by R.W.F. Gross, J.F. Bott, published by John Wiley and Sons, Inc.

/2/ K. Eidmann, Ch. Dorn, R. Sigel, IPP Report, IPP IV/95, Dez. 1976

/3/ G. Brederlow, PLF Report, PLF 5, 1978

/4/ F.C. Jahoda, E.M. Little, W.E. Quinn, G.A. Sawyer, T.F. Stratton, Phys. Rev. Vol. 119, 843, 1960

/5/ R.P. Godwin, R. Sachsenmaier, R. Sigel, Phys. Rev. Lett. Vol 39, 1198, 1977

/6/ R.P. Godwin, C.G.M. van Kessel, J.N. Olsen, P. Sachsenmaier, R. Sigel, K. Eidmann, Z. Naturforsch. Vol. 32a, 1100, 1977

/7/ B.H. Ripin, Appl. Phys. Lett., Vol. 30, 134, 1977

/8/ R. Sigel, 3. Intern. Congr. on Waves and Instabilities, June 27 - July 1, 1977, Palaiseau/France, published in Journal de Physique Vol. 38, C 6-35, 1977

/9/ K. Eidmann, M.H. Key, R. Sigel, J. Appl. Phys. Vol. 47, 2402, 1976

/10/ D.W. Forslund, J.M. Kindel, K. Lee, Phys. Rev. Lett. Vol. 39, 284, 1977

/11/ The values for T_{hot} presented at the 11th Eur. Conf. on Las. Int. with Matter in Oxford were lower since at that time the finite scintillator thickness was not taken into account.

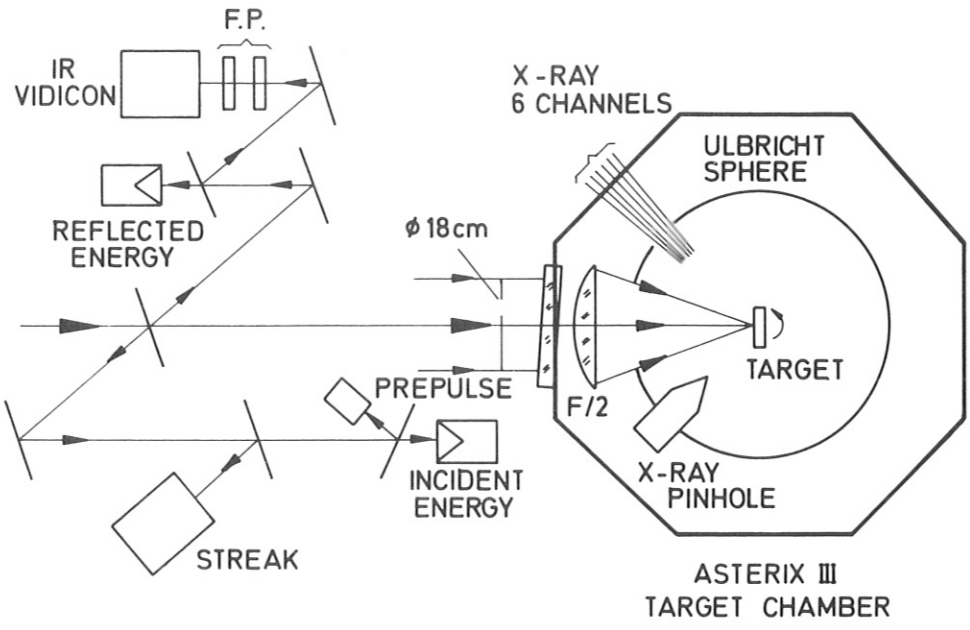

Fig. 1 Scheme of the diagnostics used for target experiments

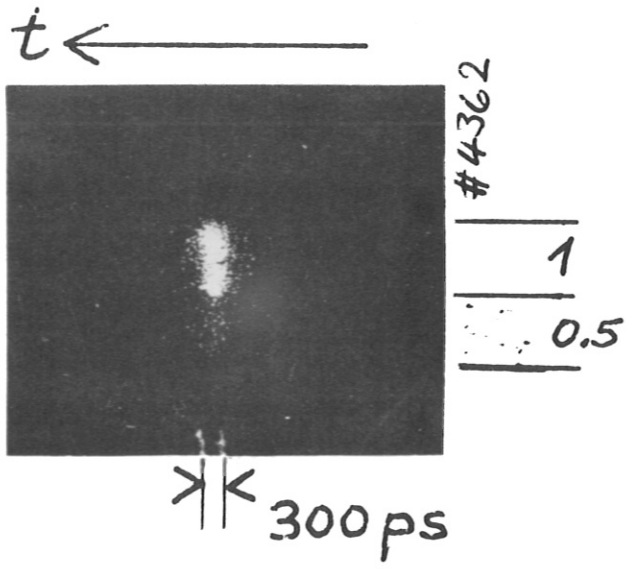

Fig. 2 Streak-picture of the laser pulse. One half of the streak slit was covered with a 50% filter.

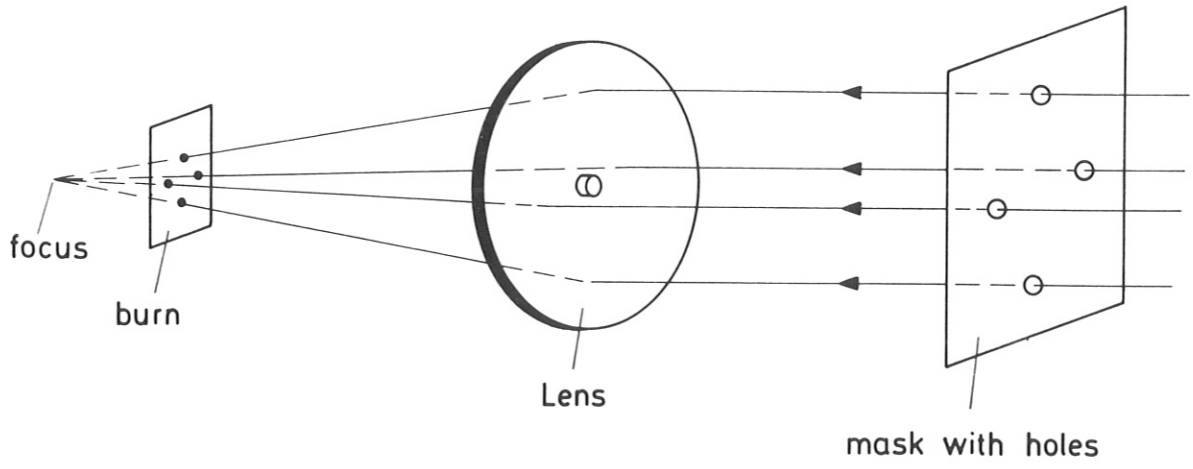

Fig. 3 Measurement of the axial focus position

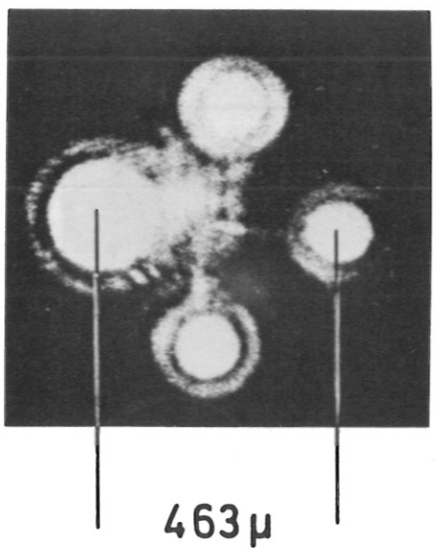

Fig. 4 Burn made near focus using the setup of fig. 3

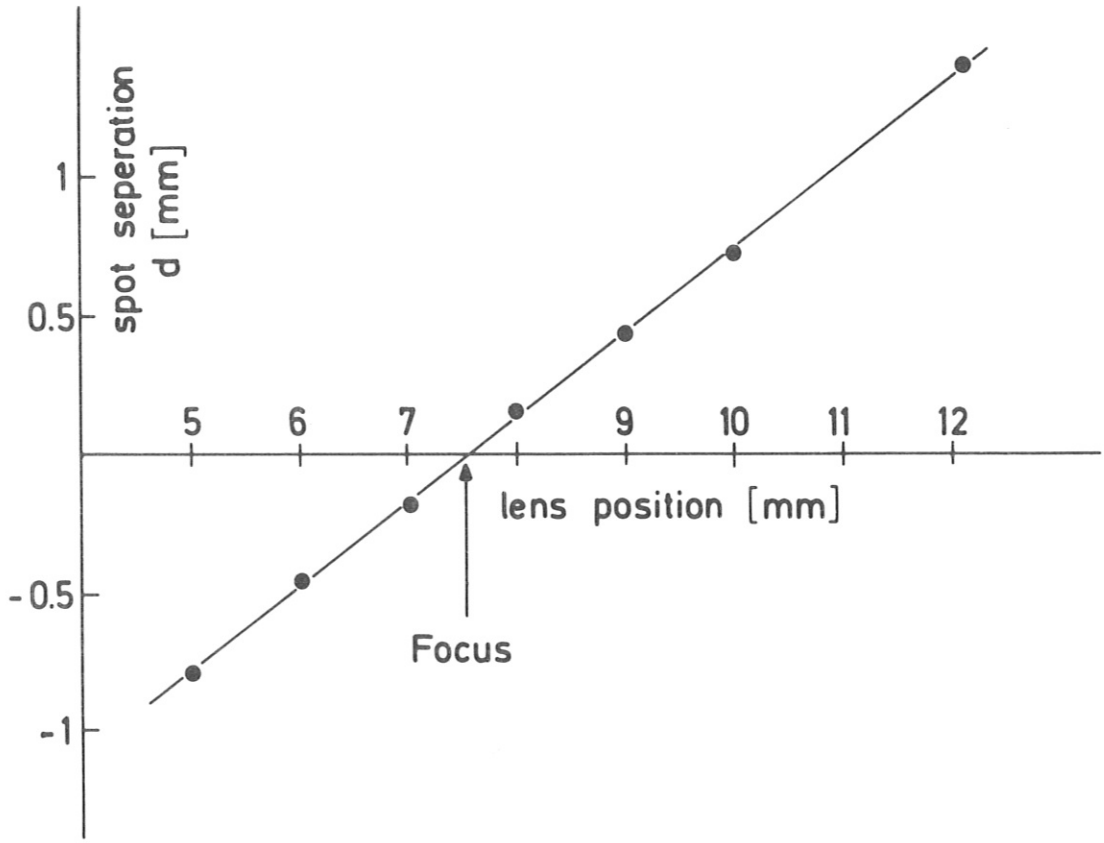

Fig. 5 Spot separation as a function of the lens position

CRATER WITH ASTERIX III

STEELTARGET

INCIDENT ENERGY ≈ 30 J (300 ps)

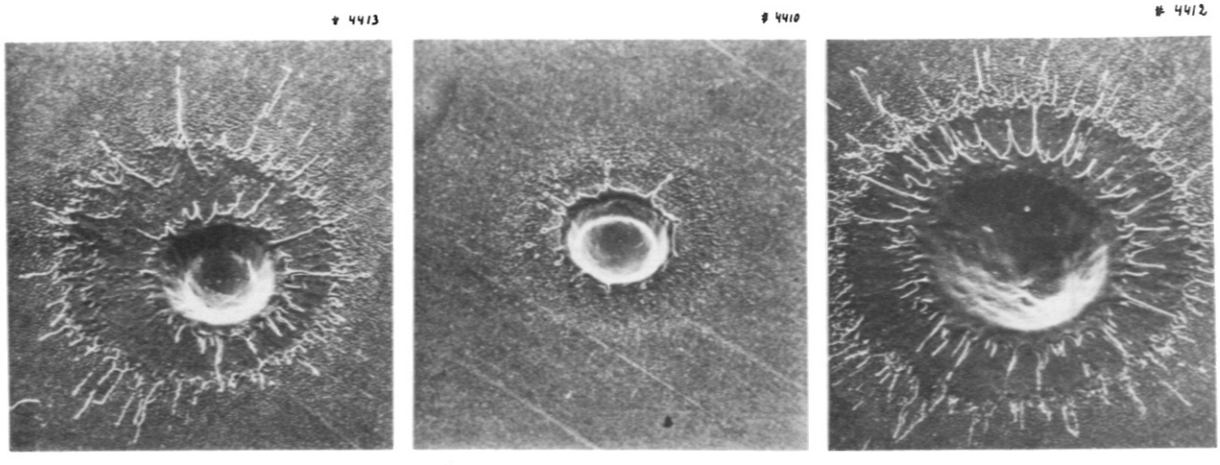

FOCUS 300 µm IN FRONT OF TARGET

FOCUS ON TARGET

FOCUS 300 µm INSIDE

Fig. 6 Craters produced on a steel-target with Asterix III

CRATER WITH YAG LASER

STEELTARGET

INCIDENT ENERGY ≈ 350 mJ (10 ns)

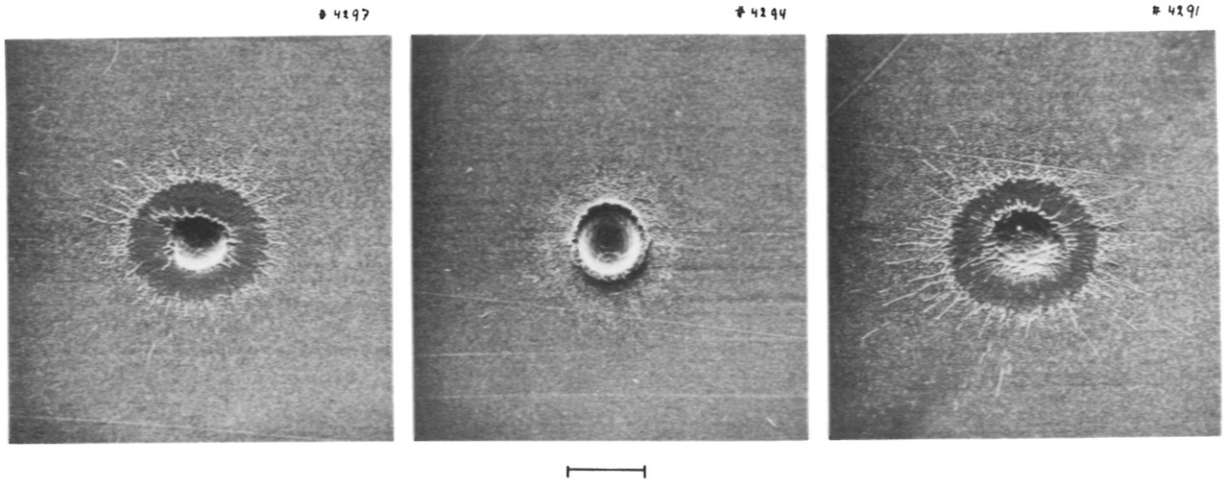

FOCUS 300 µm IN FRONT OF TARGET

FOCUS ON TARGET

FOCUS 300 µm INSIDE

Fig. 7 Craters produced on a steel-target with a Yag-laser

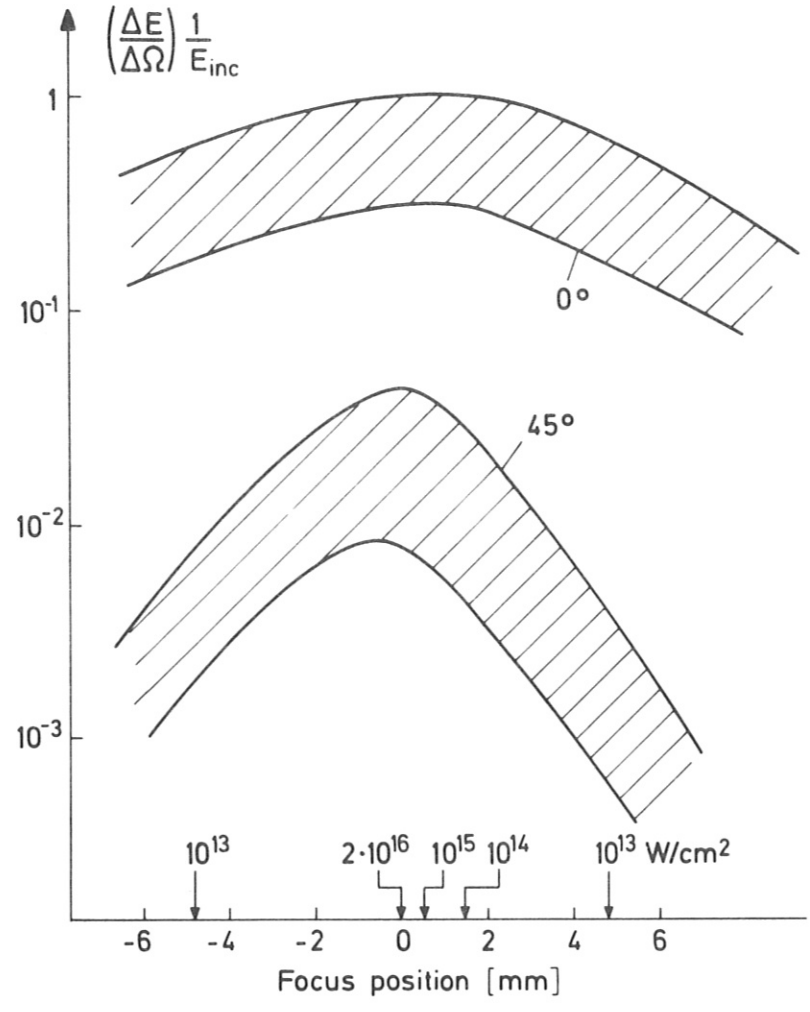

Fig. 8 Intensity scattered into the focussing lens (ϑ = 0°) and into a lens viewing under 45° to the laser axis

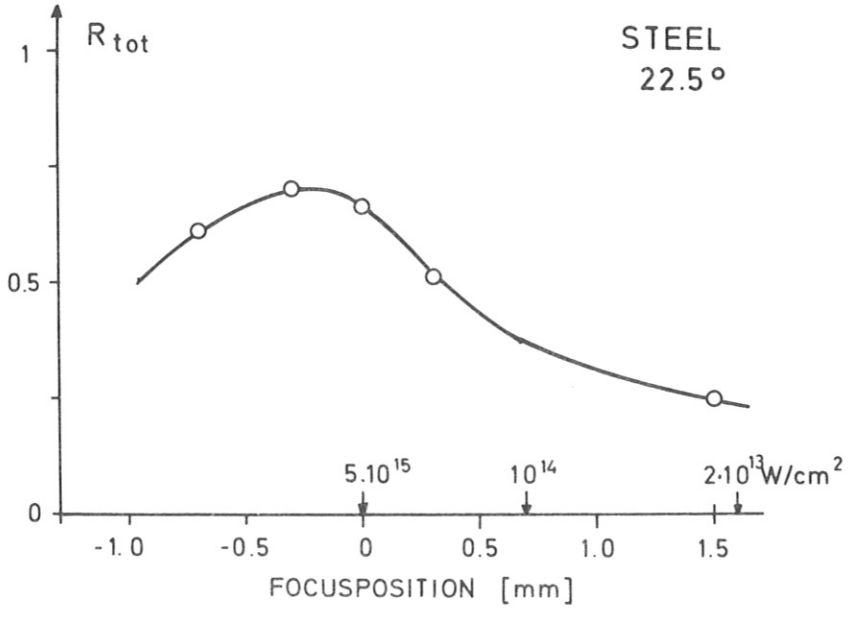

Fig. 9 Total reflection for different focus positions

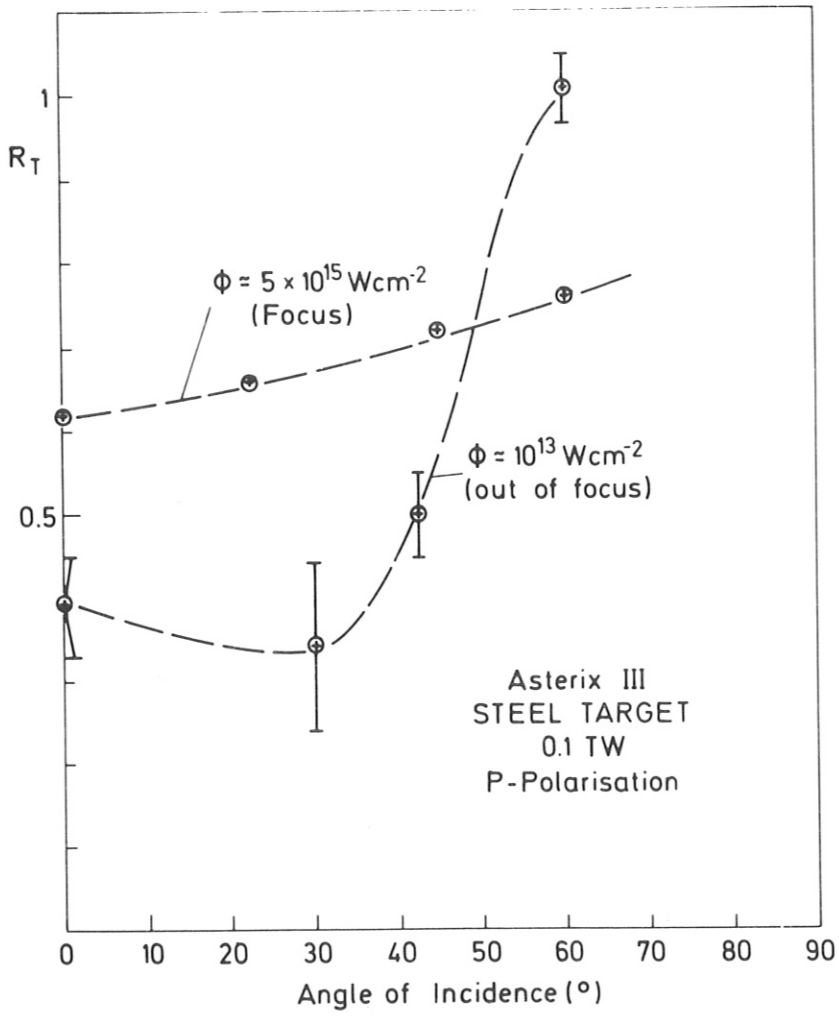

Fig. 10 Total reflection as a function of the angle of incidence for two different focus positions. The points for the in-focus-curve are due to single shots, the points of the out-of-focus-curve represent an average of about 3 shots.

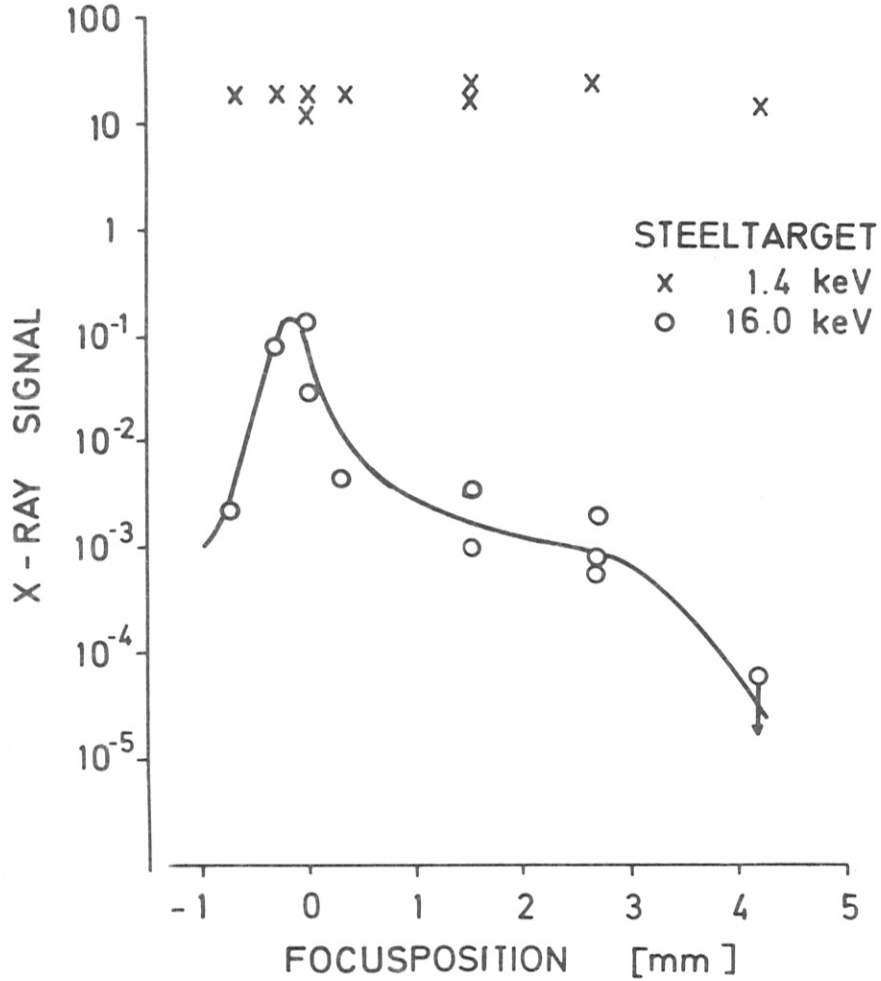

Fig. 11 Soft and hard X-ray signal for different focus positions.

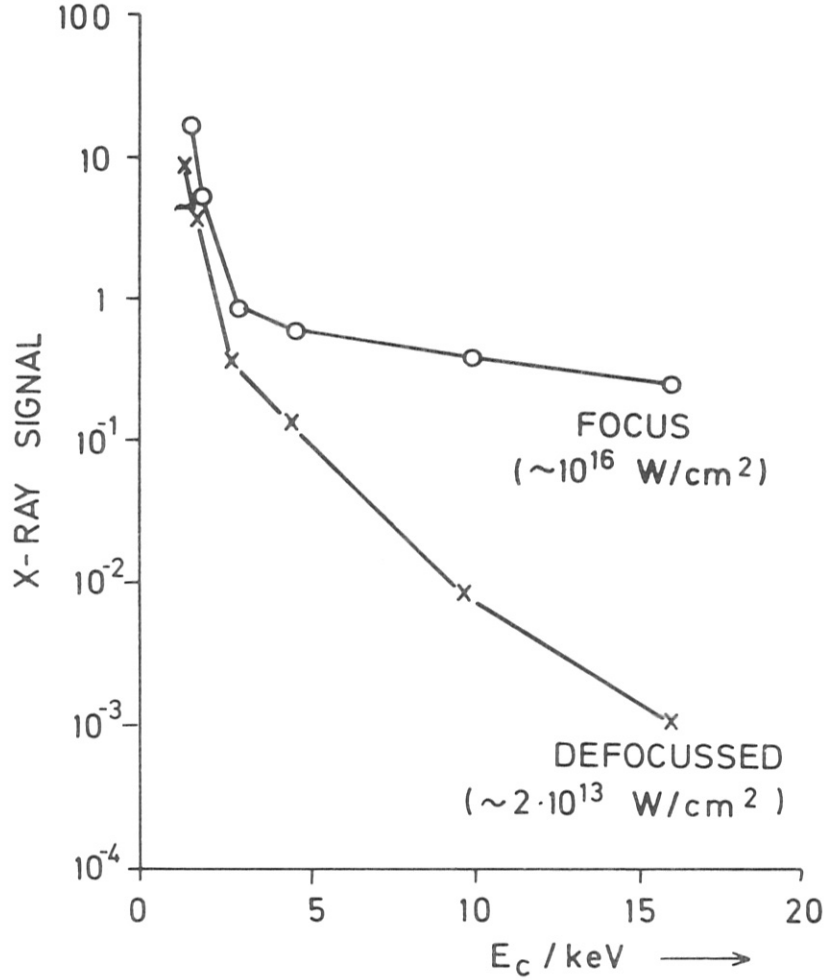

Fig. 12 X-ray signals of different absorber foils

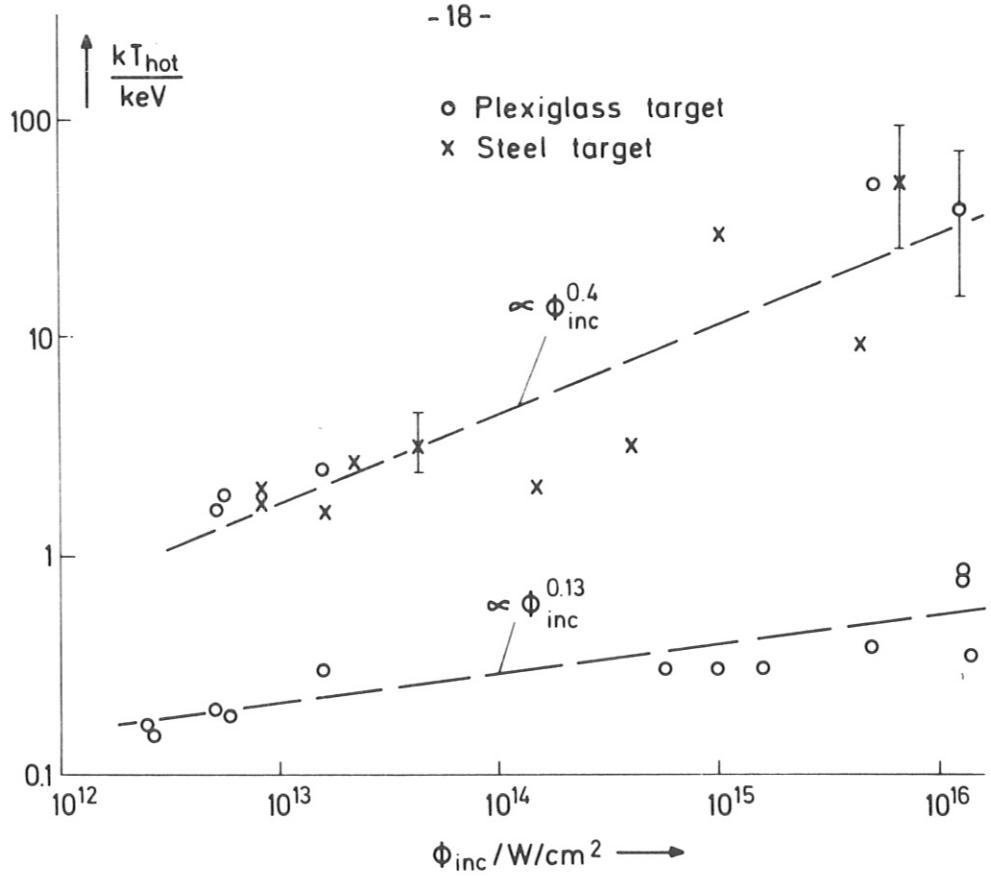

Fig. 13 Hot and cold electron temperature as a function of the incident laser intensity

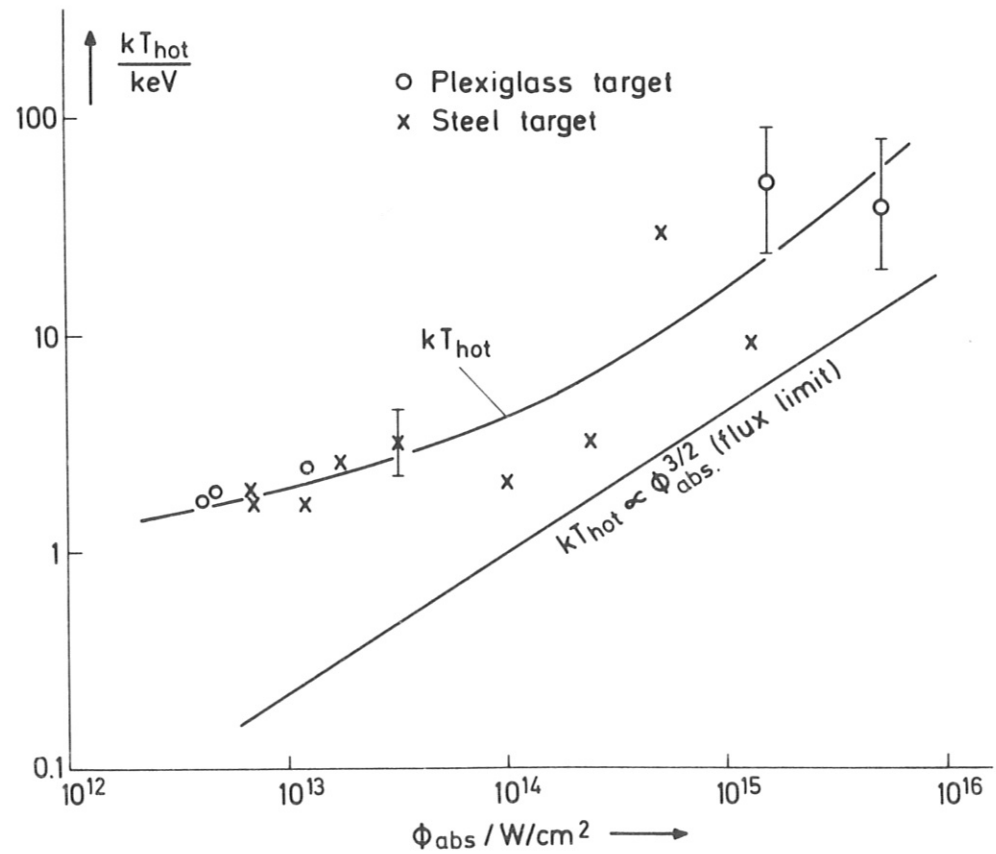

Fig. 14 kT_{hot} as function of the absorbed intensity. In addition, kT_{hot} calculated from the flux limit, see text, is plotted.

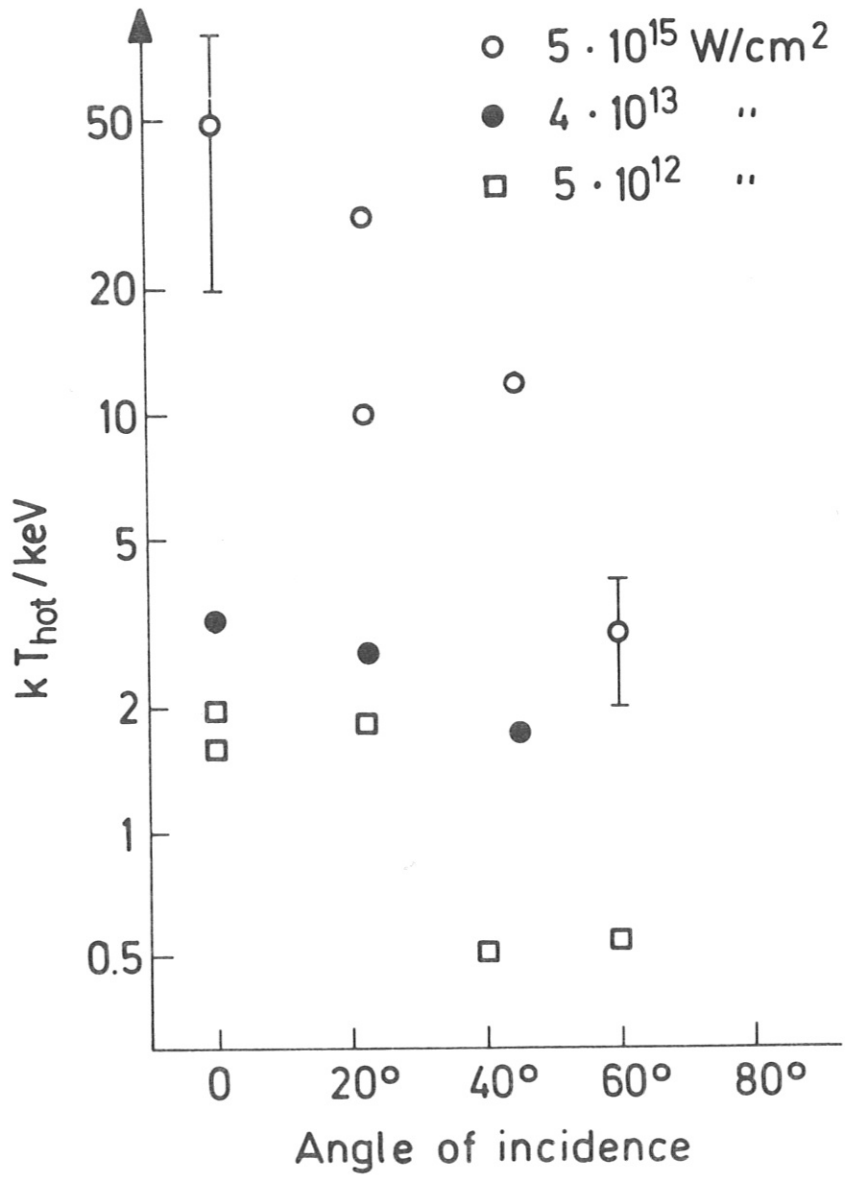

Fig. 15 kT_{hot} as a function of the angle of incidence for 3 different focus positions.